Structural basis for activation of the autoinhibitory C-terminal kinase domain of p90 RSK2

Margarita Malakhova, Valentina Tereshko, Sung-Young Lee, Ke Yao, Yong-Yeon Cho, Ann Bode, Zigang Dong

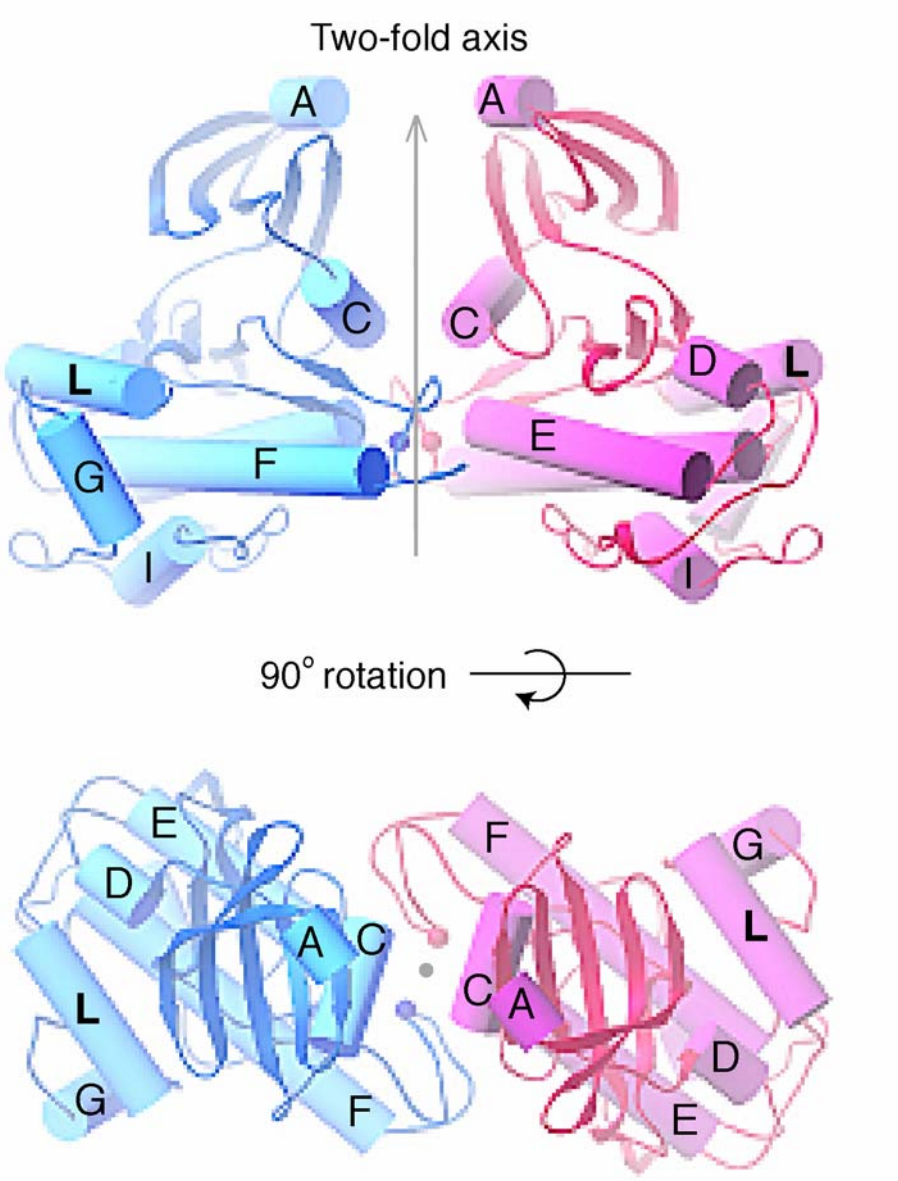


**Supplementary Figure 1.** Two perpendicular views of the crystallographic dimer. Crystal packing results in a dimer formation through T-loop residues 569-585, whereas in solution the CTD exists as a monomer (**Supplementary Methods**). In the crystals the dimer is stabilized by the disulfide bond formed between the Cys579 residues (shown as a small spheres) of two symmetry-related molecules.

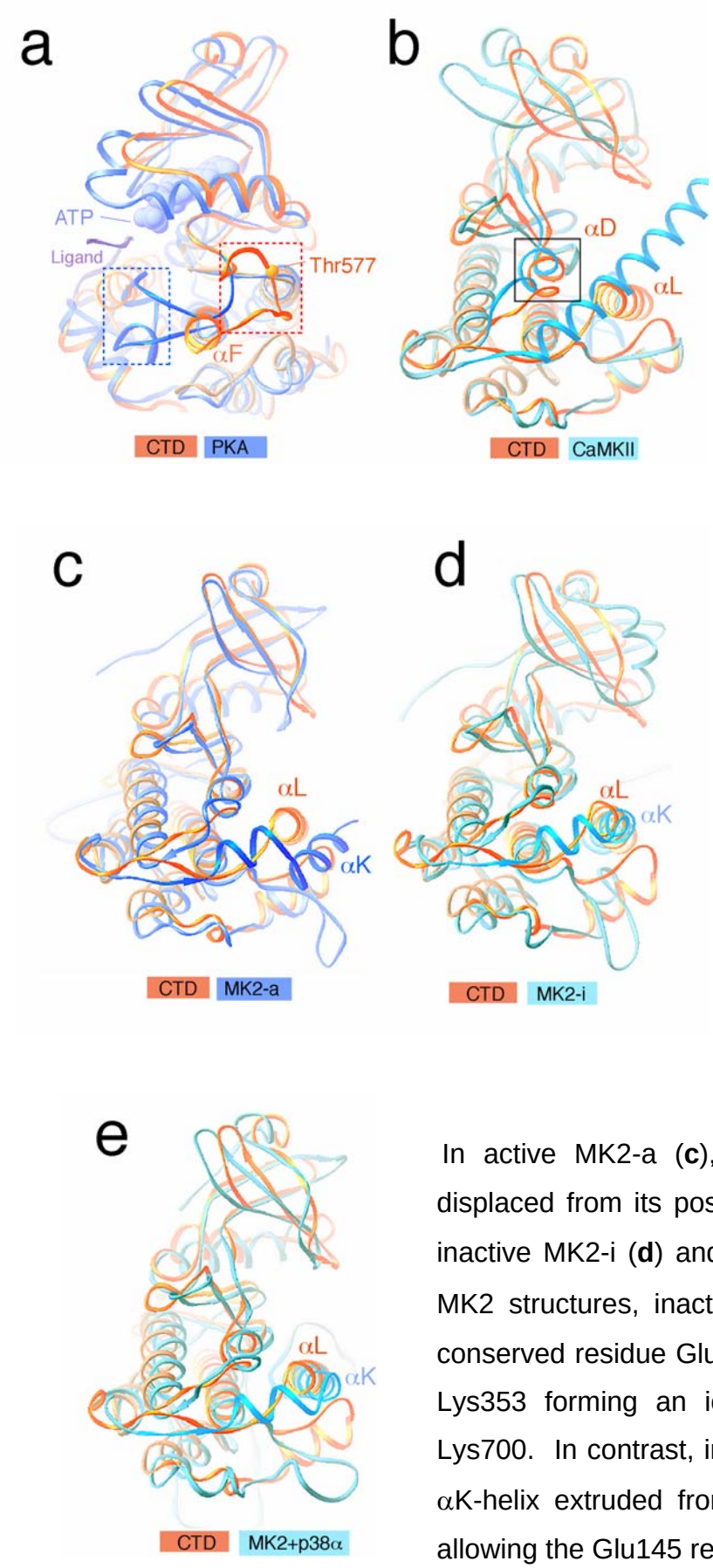


**Supplementary Figure 2.** The CTD RSK2 superposition with the selected kinases**.** (**a**) The active PKA (chain A, PDB 1CDK). The CTD T-loop residues 579-585 and the adjacent αF-helix residues 586-590 (in gold) are partially disordered in most of the crystals tested, which suggests flexibility of that region in solution and refolding upon phosphorylation. The comparison of CTD and PKA structures suggests that the αL-helix displacement might be associated with the rearrangement of the phosphorylated T-loop and its reposition in the front of the catalytic cleft. (**b**) The autoinhibited $Ca^{2+}$/calmodulin-dependent kinase CaMKII, PDB 2BDW. (**c**) MAPK-activated protein kinase 2 (MK2) crystallized in the constitutively active conformation[13] - MK2-a, PDB ID 1NXK, chain C. (**d**) MK2 in an inactive conformation[14] - MK2-i, PDB 1KWP. (**e**) MK2 in the complex with p38α[15] - MK2+p38α, PDB 2OZA.

In active MK2-a (**c**), the autoinhibitory C-terminal αK-helix is displaced from its position underneath the catalytic cleft found in inactive MK2-i (**d**) and in MK2 complexed with p38α (**e**). In both MK2 structures, inactive (**d**) and complexed with p38α (**e**), the conserved residue Glu145 is involved in the ionic interactions with Lys353 forming an ionic pair analogous to the CTD Glu500-Lys700. In contrast, in MK2-a structure (**c**) with the autoinhibitory αK-helix extruded from a "cradle" the αD-helix is free to move allowing the Glu145 readjustment toward the ATP binding site.

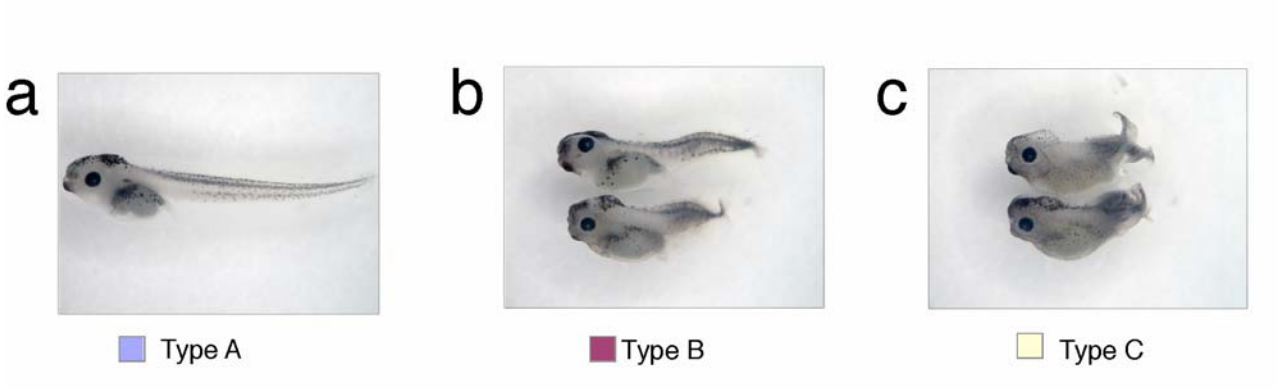


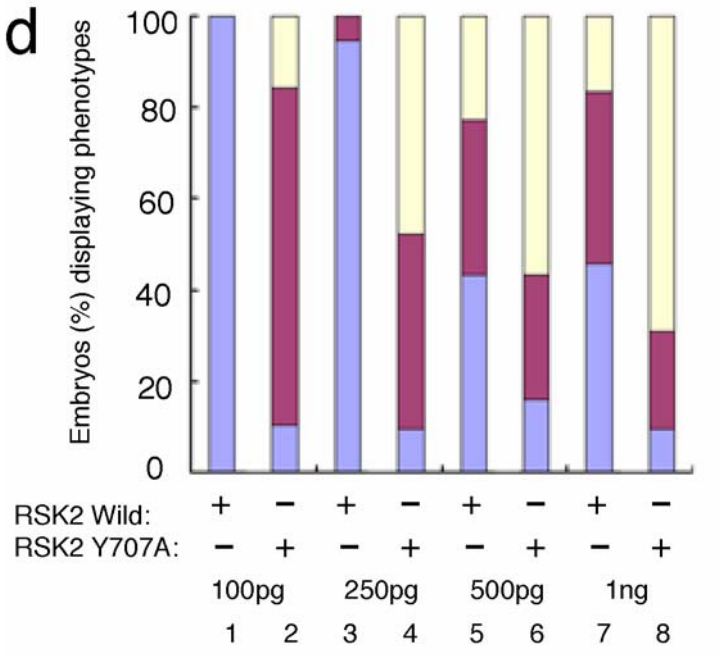


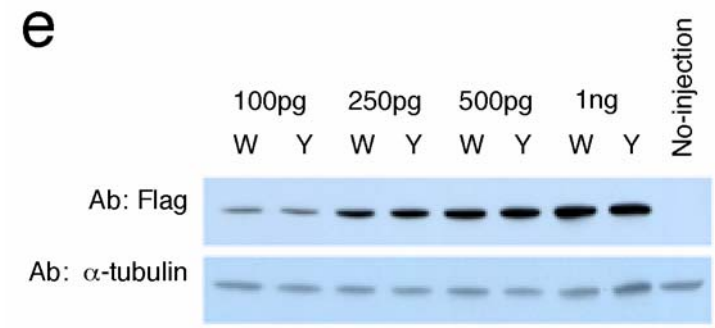


**Supplementary Figure 3.** Enhanced Y707A RSK2 activity in *Xenopus* embryos. (**a**) Example of a normal embryo (Type A) after injection with the mRNA of β-galactosidase (1 ng) as a control. Example of phenotype deformity, Type B (**b)** and Type C (**c**) induced by injection with mRNA of RSK2 wild type or the Y707A RSK2 at various concentrations. Both embryo types exhibited anterior-posterior axis (A-P axis) defects. (**d**) Histogram showing the occurrence of Type A, B, and C embryos after injection with various amounts (100 pg-1 ng) of mRNA of the wild type RSK2 or mutant Y707A RSK2. These data are representative of at least three independent experiments. The mutant Y707A RSK2 induced a phenotypic change that was more severe than that induced by wild type RSK2 expression. The injection of wild type RSK2 mRNA at 100 pg did not induce a phenotypic change (lane 1), whereas injection of an equivalent amount of mutant Y707A RSK2 mRNA resulted in an A-P axis defective phenotype (Type B or C) in most of the embryos (~90%) (lane 2). (**e**) Western blot analysis demonstrated that approximately similar amounts of the wild type (W) or Y707A mutant (Y) forms of RSK2 are expressed in the embryos when an equivalent amount of RNA (100 pg – 1ng) is introduced.

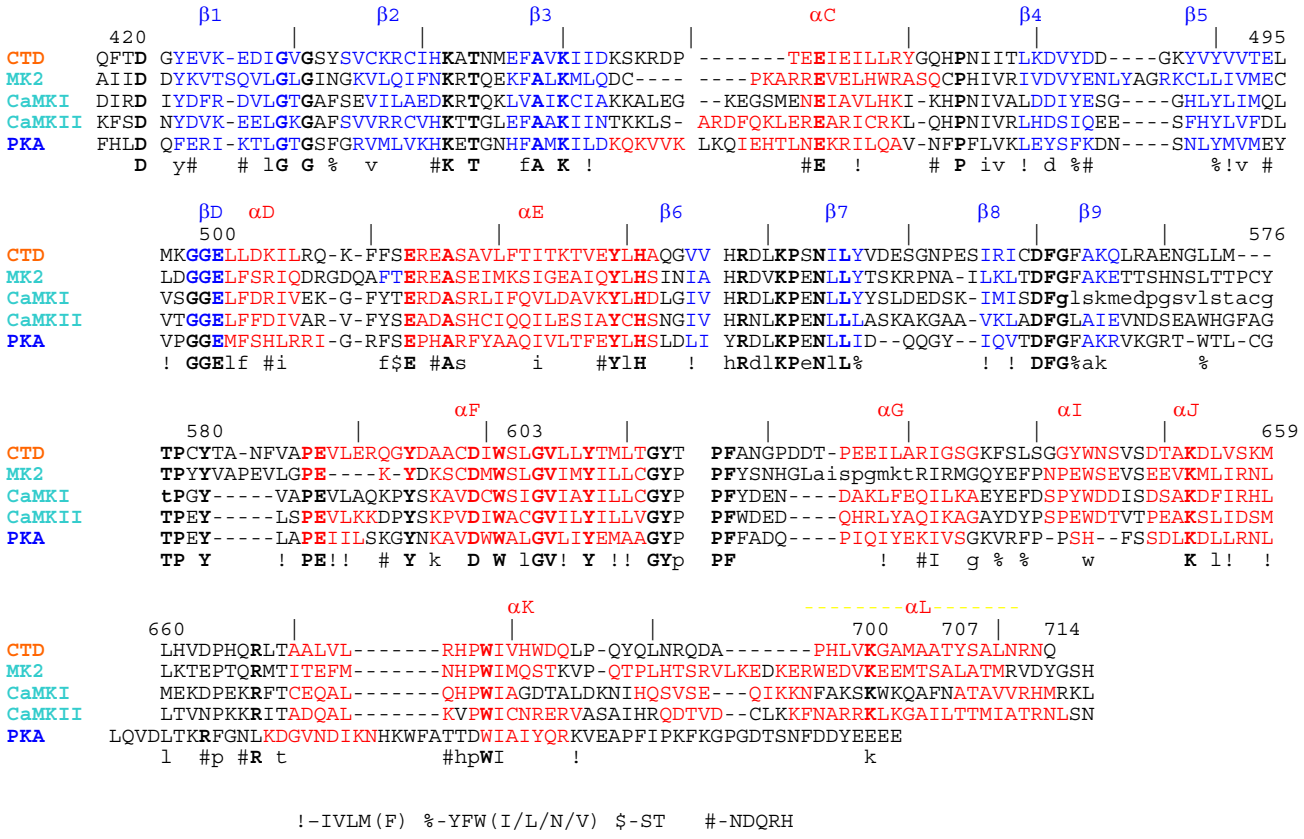


**Supplementary Figure 4.** Sequence alignment based on the secondary structure determined by X-ray crystallography. Secondary structure elements of aligned sequences are numbered and are highlighted with colors that match those in the folding diagram of **Fig.1a**. The CTD residue numbering (with each 10th residue shown with a vertical line) is below the secondary structure diagram. Amino acids conserved in five kinases are shown in bold. Insertions/deletions in kinase sequences are shown as dashed lines. The residues that are disordered in the crystal structures are shown in lower case letters. The CTD RSK2 N-terminal residues 399-410 and C-terminal residues 715-440, which are disordered in the crystal structure, are omitted from the alignment.

**Supplementary Table 1. X-ray data collection and refinement statistics[a)]**

| | Se-Met derivative | Native |
|---|---|---|
| **Data collection** | | |
| Space group | $P4_12_12$ | $P4_12_12$ |
| Cell dimensions | | |
| *a*, *b*, *c* (Å) | 46.59, 46.59, 293.99 | 46.91, 46.91, 291.08 |
| $\alpha, \beta, \gamma$ (º) | 90, 90, 90 | 90, 90, 90 |
| Resolution[b)] (Å) | 50-2.0 (2.06-2.0) | 50-2.0 (2.06-2.0) |
| $R_{merge}$ | 0.079 (0.44) | 0.08 (0.47) |
| $I/\sigma I$ | 36.9 (6.0) | 30.6 (3.0) |
| Completeness (%) | 99.9 (100) | 98.8 (99.0) |
| Redundancy | 7.7 (7.1) | 5.5 (5.3) |
| | | |
| **Refinement** | | |
| Resolution (Å) | 20 – 2.0 | 20 – 2.0 |
| No. reflections | 23160 | 23175 |
| $R_{work}$/ $R_{free}$ | 0.202 / 0.237 | 0.217 / 0.256 |
| No. atoms | | |
| Protein | 2340 | 2361 |
| Ions | 1 Na | 1 Na |
| Water | 91 | 77 |
| B-factors | | |
| Protein | 44.9 | 53.0 |
| Ions | 42.3 | 48.4 |
| Water | 46.8 | 54.3 |
| R.m.s deviations | | |
| Bond lengths (Å) | 0.012 | 0.013 |
| Bond angles (º) | 1.21 | 1.23 |

[a)] One SeMet labeled and one native crystal was used for the structure determination.
[b)] Highest resolution shell is shown in parenthesis.

## Materials and Methods

**Protein purification and crystallization.** The CTD of murine RSK2 (residues 399-740) was subcloned into the pET-46 EK/LIC vector (EMD Chemicals, Inc., Can Diego, CA) and expressed in *E.coli* BL21-Codon Plus (DE3)-RILP (Stratagene, La Jolla, CA) competent cells. Soluble His-tagged CTD RSK2 was purified on nickel-nitriloacetic acid agarose (Qiagen, Valencia, CA), and treated with enterokinase to remove the His-tag. Untagged protein was eluted as a monomer on a HiLoad 16/60 Superdex-200 size-exclusion chromatography column (GE Healthcare, Piscataway, NJ). Selenomethionine-labeled protein (SeMet) was obtained by standard procedures[1]. Several crystallization conditions were determined with Index crystallization screening (Hampton Research, Aliso Viego, CA) and optimized. The protein samples (5-13 mg/ml in the presence of 10 mM β-mercaptoethanol) were mixed with an equal volume of precipitant that contained 7.5%–10% polyethylene glycol 3350, 50 mM ammonium sulfate, and 0.1 M Hepes (pH 7.0). Crystal soaking and co-crystallization trials in the presence of the non-hydrolyzable ATP analogue, AMP-PNP and $MgCl_2$ were performed using a broad range of incubation and co-crystallization conditions. All obtained crystals were cryo-protected in mother liquor with 20% ethylene glycol and flash-frozen in liquid nitrogen.

**Data collection and structure determination.** The SeMet labeled and native CTD RSK2 crystals were isomorphous and belonged to the $P4_12_12$ space group. Single-wavelength anomalous dispersion (SeMet labeled protein, Se-edge energy, $\lambda$=0.97936 Å) and native ($\lambda$=0.97950 Å) X-ray data sets were collected at 100K at Advanced Photon Source (Argonne National Laboratory) using the 23ID-D and 24ID-C beam lines, respectively. Both X-ray data

sets were collected using 280 mm crystal-to-detector distance, 0.5˚ oscillation width and 2 sec exposure time. Images were processed and scaled with HKL2000[2].

The structure was solved by SAD technique on SeMet labeled crystals. A heavy atom search was performed in SHELXD[3] using X-ray data collected at peak energy and 3.5 Å resolution cut-off. SAD phasing and density modification were performed with the use of the SOLVE/RESOLVE suite[4]. The model building performed with the RESOLVE basic script was completed using the ARP/wARP program[5]. The electron density and model examinations were performed using TURBO-FRODO[6]. The restrained positional and isotropic B-factor refinement was done in REFMAC5[7]. R-free was monitored by setting aside 5% of the reflection as a test set. Crystal data, X-ray data collection and refinement statistics are listed in Table 1. A Ramachandran plot calculated with PROCHECK[8] indicated that 93.1% and 6.9% of the non-Gly and non-Pro residues in the final models lie in the most favored and additional allowed regions, respectively. The surface area calculations were performed using Protein-Protein Interaction Server (http://www.biochem.ucl.ac.uk/bsm/PP/server). The three-dimensional figures were prepared with the use of RIBBONS[9]. The potential surface was prepared with GRASP[10]. All numbering of amino acid residues is according to full length murine RSK2.

***Xenopus* experiments.** Mouse RSK2 full length or the Y707A mutant plasmid was inserted into a BglII/XbaI digested pCS2-flag tagged vector. mRNA synthesis and microinjection were performed as previously described[11,12]. Fertilized eggs were injected in the animal pole with messenger RNA at the one-cell stage. The embryos were then cultured for 3 or 4 day in 30% Modified Frog Ringers (MR) buffer comprised of 0.1 M NaCl, 2 mM KCl, 2 mM $CaCl_2$, 1 mM $MgCl_2$, 5 mM HEPES, pH 7.6. The embryos, which were cultured until stage 40, were rinsed

several times with 1X PBS, fixed for one hour at room temperature in MEMFA (0.1 M MOPS, 2 mM EGTA, 1 mM $MgSO_4$, 3.7% formaldehyde), and stored at 4°C in 100% methanol. Fixed embryos were observed and photographed under a microscope. An anti-Flag antibody (Sigma-Aldrich, St. Louis, MO) was used for the detection of the equivalent expression of RSK2 by Western blot analysis. Detection of α-tubulin was used as a loading control.

**Supplementary References**


1. Doublie, S. Preparation of Selenomethionyl Proteins for Phase Determination. *Methods in Enzymology* **276**, 523-530 (1977).
2. Otwinowski, Z., Minor, W. Processing of x-ray diffraction data collected in oscillation mode. *Methods in Enzymology* **276**, 307-326 (1997).
3. Schneider, T.R., Sheldrick, G.M. Substructure solution with SHELXD. *Acta Crystallogr. D Biol. Crystallogr.* **58**, 1772-1779 (2002).
4. Terwilliger, T.C., Berendzen, J. Automated MAD and MIR structure solution. *Acta Crystallogr., D Biol. Crystallogr.* **55**, 849-861 (1999).
5. Lamzin, V.S., Perrakis, A., Wilson, K.S. *The ARP/WARP suite for automated construction and refinement of protein models. In Int. Tables for Crystallography*, 720-722 (Dordrecht, Kluwer Academic Publishers, The Netherlands, 2001).
6. Cambillau, C., Roussel, A. Turbo Frodo, version OpenGL.1. in *University Aix-Marseille II: marseille* (1997).
7. Murshudov, G.N., Vagin, A.A., Dodson, E.J. Refinement of macromolecular structures by maximum-likelihood method. *Acta Crystallogr., D Biol. Crystallogr.* **53**, 240-255 (1997).

8. Laskowski, R.A., MacArthur, M.W., Moss, D.S., Thornton, J.M. PROCHECK: a program to check the stereochemical quality of protein structures. *J. Appl. Cryst.* **26**, 283-291 (1993).

9. Carson, M. Ribbons. *Methods in Enzymology* **277**, 493-505 (1996).

10. Nicholls, A., Sharp, K.A., Honig, B. Protein folding and association: insights from the interfacial and thermodynamic properties of hydrocarbons. *Proteins* **11**, 281-296 (1991).

11. Dong, Z. *et al*. AP-1/jun is required for early Xenopus development and mediates mesoderm induction by fibroblast growth factor but not by activin. *J. Biol. Chem*. **271**, 9942-9946.

12. Xu, R. H. *et al*. Involvement of Ras/Raf/AP-1 in BMP-4 signaling during Xenopus embryonic development. *Proc. Natl. Acad. Sci. USA* **93**, 834-838 (1996).

13. Underwood, K.W. *et al.* Catalytically active MAP KAP kinase 2 structures in complex with starosporine and ADP reveal differences with the autoinhibited enzyme. *Structure* **11**, 627-636 (2003).

14. Meng, W. *et al*. Structure of mitogen-activated protein kinase-activated protein (MAPKAP) kinase 2 suggests a bifunctional switch that couples kinase activation with nuclear export. *J.Biol.Chem.* **277**, 37401-37405 (2002).

15. White, A., Pargellis, C.A., Studts, J.M., Werneburg, B.G., Farmer II, B.T. Molecular basis of MAPK-activated protein kinase 2:p38 assembly. *PNAS* **104**, 6353-6358 (2007).